



RESEARCH ARTICLE

Comparison of extreme temperature response to 0.5 °C additional warming between dry and humid regions over East–central Asia

Meng Zhang¹  | Haipeng Yu^{1,2} | Jianping Huang¹ | Yun Wei¹  | Xiaoyue Liu¹ | Tinghan Zhang¹

¹Key Laboratory for Semi-Arid Climate Change of the Ministry of Education, College of Atmospheric Sciences, Lanzhou University, Lanzhou, China

²Key Laboratory of Arid Climate Change and Reducing Disaster of Gansu Province, Key Open Laboratory of Arid Climate Change and Disaster Reduction of CMA, Institute of Arid Meteorology, China Meteorological Administration, Lanzhou, China

Correspondence

Haipeng Yu, Key Laboratory for Semi-Arid Climate Change of the Ministry of Education, College of Atmospheric Sciences, Lanzhou University, Lanzhou, China.
Email: hpyu09@lzu.edu.cn

Funding information

China Postdoctoral Science Foundation, Grant/Award Number: 2017M613250; National Key Research and Development Program of China, Grant/Award Number: 2017YFC1502305; National Natural Science Foundation of China, Grant/Award Numbers: 41705077, 41630426

The additional 0.5 °C warming from 1.5 to 2°C global target has a significant impact on the occurrence of extreme temperature events. While the arid and semi-arid areas (ASA) and humid areas (HA) present different response characteristics to the additional global mean 0.5 °C warming due to their differences in thermal properties. In this study, both the stabilized and transient 1.5 °C (2 °C) global warming scenarios projected by the Community Earth System Model (CESM) are used to compare the extreme temperature responses between the ASA and HA to the 2 and 1.5 °C global warming targets over East–central Asia. The results indicate that cold fixed-threshold indices (frost days [FD] and icing days [ID]) will decrease more rapidly in ASA, by approximately 10 days (1.5 °C) and 15 days (2 °C) compared to the historical period, respectively. Warm fixed-threshold indices (summer days [SU] and tropical nights [TR]) will become more common in HA, especially southeast of China. Under 1.5 °C target, the increase of intensity indices is equal to the average temperature warming response (1.5 °C), while the additional 0.5 °C warming makes the response of intensity indices much greater than 0.5 °C. Under 0.5 °C warmer world, the daily temperature range (DTR) will experience a 0.5 °C increase in most HA and a 0.2–0.5 °C decrease in ASA during winter. As a whole, the additional 0.5 °C warming has an amplified effect and the 1.5 °C global warming target could reduce the extreme temperature events significantly over East–central Asia.

KEYWORDS

additional 0.5 °C warming, arid and semi-arid areas, East–central Asia, extreme temperature indices, humid areas

1 | INTRODUCTION

Since the 2015 Paris Agreement, 1.5 and 2 °C warming targets have gradually become a consensus that should be observed and supported by governments and the public all over the world. Global climate change and its impact on socioeconomic development, environment, and our everyday lives under those warming conditions have been thoroughly addressed by voluminous literature (Guiot and Cramer, 2015; van Hooidek *et al.*, 2016; James *et al.*, 2017; Kraaijenbrink *et al.*, 2017; Huang *et al.*, 2017a). However, most scholars focus on regional mean temperature change, sea

level rise, Arctic sea ice melting, and many other slow change processes (Serreze and Stroeve, 2015; Schleussner *et al.*, 2016; Chen *et al.*, 2017; Oliva *et al.*, 2017). In the meanwhile, rapid processes such as extreme high- or low-temperature events, storms, typhoons, and some other meteorological disasters should not be neglected (Guo *et al.*, 2016; Nangombe *et al.*, 2018). Some scholars have made great contributions to analysing extreme climate change in certain specified global warming targets. Note that most previous studies concentrated on the spatiotemporal changes of major climate extremes themselves (e.g., heatwaves and floods). For instance, larger anomalies in climate extreme

indices are projected to be found at 3 °C than that at 2 and 1 °C (Chen and Sun, 2014), and an additional 0.5 °C warming increasing from 1.5 to 2 °C would induce more precipitation extremes in China (Wang *et al.*, 2017; Li *et al.*, 2018; Lin *et al.*, 2018). India is more likely to expose in severe heatwaves if global temperature exceeds 1.5 °C (Mishra *et al.*, 2017). Besides East and South Asia, more climate extremes are projected to occur in Australia due to an additional 0.5 °C warming (King *et al.*, 2017). Some other studies have been performed to investigate the associated impacts brought by extreme climate changes (e.g., river flows and human health). They pointed out that more people are threatened by extreme precipitation and extreme flows in several large catchments, which are projected to increase the occurrence frequency under 2 °C limits relative to 1.5 °C (King *et al.*, 2018; Paltan *et al.*, 2018). To sum up, all their researches indicated that in the warming future, climate extremes will increase in intensity, frequency, and duration. Moreover, related potential risks will be higher along with the temperature increase. In our study, the comparison of arid and semi-arid areas (ASA) and humid areas (HA) in East and central Asia should be highlighted due to their significant differences in responding to extreme temperature in the warming future and the lack of associated study.

Although clarifying the mechanisms of extreme temperature events is quite difficult at the present stage, it is crucially important to evaluate the risks of extreme temperature events under a global warming background (Coumou and Rahmstorf, 2012). As a usual and destructive extreme climate event, this continuing temperature anomaly could cause dramatic damage manifested by both casualties and property loss (Cattiaux *et al.*, 2010; Barriopedro *et al.*, 2011; Dole *et al.*, 2011; Otto *et al.*, 2012; Peterson *et al.*, 2013; Agha-Kouchak *et al.*, 2014). Since the beginning of the millennium, the occurrence of many record-breaking events awakened humans to the reality of climate change. As an example (You *et al.*, 2011; Chen and Sun, 2015), China sustained high temperatures that resulted in heatwaves and drought disasters in most parts of the country in 2000 and 2001; the affected area had been the largest since 1950. In 2010, southwestern areas of China witnessed a major drought caused by temperature anomalies, lack of precipitation, and El Niño. In the meanwhile, the intensity and duration of cold events has been reduced. Nevertheless, severe cold events and their derivative disasters such as the snow disaster in 2008 still caused major losses to the Chinese society and economy.

East-central Asia is a sensitive and vulnerable region due to the significant sea-land thermal differences and complex terrain conditions (Zhou and Zou, 2010; Li *et al.*, 2016; Xing *et al.*, 2016). Furthermore, as the surface air temperature rapidly increases, the occurrence risk of extreme temperature events also increases as well as the single event intensity (as discussed previously). Therefore, some

researchers have focused their attention on this issue and have achieved meaningful results after the Paris Agreement (Sanderson *et al.*, 2016; Sanderson *et al.*, 2017; Wang *et al.*, 2017; Chen and Sun, 2018; Dosio and Fischer, 2018; Li *et al.*, 2018a). However, precipitation and potential evapotranspiration (PET) are two important factors in extreme temperature events because they could influence temperature variability through changing latent heat flux and sensible heat flux (Wild *et al.*, 2013). For HA, the true evaporation could reflect the amount of water supply by and large. Latent heat flux contributes more to evaporation than sensible heat flux, whereas for ASA, there is far less precipitation than evaporation, which leads to a lack of moisture at the surface and in the atmosphere; therefore, sensible heat flux accounts for a higher proportion of evaporation (Fu and Feng, 2013; Wang and Dickinson, 2013; Huang *et al.*, 2016a). Moreover, dust aerosols have a warming effect within the atmosphere in Asian ASA (DeMott *et al.*, 2003; Evan *et al.*, 2009; Huang *et al.*, 2017b). Compared with water clouds, ice clouds in ASA absorb more longwave radiation and reflect less shortwave radiation. Thus, more energy is retained, which warms the atmosphere and causes a stronger greenhouse effect (Huang *et al.*, 2016b; Huang *et al.*, 2017b). In addition, because of the ecological environment in ASA is more fragile than HA, the increase in extreme climate risks will do more harm to ASA and residents even though most people populate in the HA (Reynolds *et al.*, 2007). Therefore, to better understand the mean and extreme temperature changes, the East-central Asian region could not be considered as an overall analysis. The emphasis should be on the differences between wet and dry environments. For these reasons, we used the aridity index (AI), which is defined by the ratio of annual precipitation to annual potential evapotranspiration, to divide the ASA and HA in East-central Asia (Middleton and Thomas, 1992) (see section 2 for details).

To better adapt to the needs of projecting climate change in the 1.5 and 2 °C scenarios, special experiments called low-warming runs (LWR) were released by the National Center for Atmospheric Research (NCAR). These series of experiments, which used the Community Earth System Model (CESM), included 10-member ensembles for 1.5 °C (1 pt5) warming and 2 °C (2 pt) warming, respectively (Sanderson *et al.*, 2017). In addition, we also selected the results of CESM RCP4.5 and RCP8.5 experiments for comparison to analyse their differences when reaching 1.5 and 2 °C targets.

Based on the two different model simulation methods used to achieve 1.5 and 2 °C warming targets from the CESM model simulation, we aim to preliminarily cover several topics of interest. (a) The difference between 2 and 1.5 °C warming targets regarding extreme temperature event changes both in the HA and ASA of East-central Asia. (b) The difference that the 0.5 °C change will make to decrease the risk of extreme temperature events over East-

central Asia. (c) The variations of the selected extreme temperature indices under 1.5 °C conditions over East–central Asia. (d) The difference between short-term stabilization response and transient climate response to achieve 1.5 and 2 °C warming targets.

2 | DATA AND METHODS

2.1 | Data analysis

We used the NCAR CESM model with LWR to evaluate extreme temperature indices change over East–central Asia under 1.5 and 2 °C warming targets. Besides, the RCP4.5 and RCP8.5 conditions in the CESM model were also selected for comparison. The number of runs in the CESM LWR are 10 under 1.5 and 2 warming limits, respectively. Models under the RCP4.5 scenarios are 15, and under the RCP8.5 scenarios are 30. It should be noted that the NCAR CESM LWR is identified by short-term stabilization response, which means that the output of the simulations driven with emissions stabilize the mean global warming level to a specific temperature threshold of 1.5 or 2 °C by the end of the 21st century. In contrast, RCP4.5 and RCP8.5 are characterized by transient climate responses, which only pass through 1.5 or 2 °C global warming scenarios. Because the final increase exceeds the warming targets, this response usually overestimates the temperature increase and its related influence.

We handled the 1.5 and 2 °C warming data sets as follows. (a) The daily physical quantities were selected during 1920–2100 in three scenarios, which contain the mean temperature, maximum temperature and minimum temperature. (b) For each model membership in the previously mentioned scenarios, the exact time to achieve the target temperature was calculated, and the pre-industrial period was considered to be 1850–1920. Then, based on the centres of the chosen years, we extracted 11 years (5 years at both ends) overall and calculated a running average mean. (c) The ensemble mean of these three scenarios were calculated. (d) We subtracted the historical period (mean state of 1971–2000) values for the selected extreme temperature indices.

2.2 | Extreme temperature indices

The indices used in this paper are defined by the Expert Team for Climate Change Detection Monitoring and Indices (ETCCDI; Zhang *et al.*, 2011; Perkins *et al.*, 2012; Donat *et al.*, 2013; Perkins and Alexander, 2013; Sillmann *et al.*, 2013a; 2013b; You *et al.*, 2018). These indices are calculated based on the daily maximum temperature, daily minimum temperature, daily mean temperature, and daily precipitation. A full descriptive list of these indices can be obtained from http://etccdi.pacificclimate.org/list_27_indices.shtml. These 27 indices can be divided into five

different categories (Alexander *et al.*, 2006). For extreme climate model simulations, the absolute indices which represent the maximum or minimum values within a season or year (TX_X , TN_X , TX_N , and TN_N) and the threshold indices which represent annual days over a certain threshold (frost days [FD], icing days [ID], summer days [SU], and tropical nights [TR]) could intuitively show future extreme climate features. The diurnal temperature range (DTR) is an index of great concern; it could make a real difference in the growth of crops and health of humans. These indices mentioned above could help to better project extreme temperature changes. More details on the selected extreme temperature indices are provided in Table 1.

2.3 | Research area selection

We chose a 10°–55°N and 60°–150°E latitude and longitude range as our research area (not including oceans), which

TABLE 1 Core set of selected nine extreme indices recommended by the ETCCDI

Label	Name	Definition	Units
FD	Frost days	Let TN be the daily minimum temperature on day i in period j . Count the number of days where $TN_{ij} < 0^\circ\text{C}$	days
ID	Icing days	Let TX be the daily maximum temperature on day i in period j . Count the number of days where $TX_{ij} < 0^\circ\text{C}$	days
SU	Summer days	Let TX be the daily maximum temperature on day i in period j . Count the number of days where $TX_{ij} > 25^\circ\text{C}$	days
TR	Tropical nights	Let TN be the daily minimum temperature on day i in period j . Count the number of days where $TN_{ij} > 20^\circ\text{C}$	days
TX_X	Max maximum temperature	Let TX_X be the daily maximum temperature in month k , period j . The maximum daily maximum temperature each month is then: $TX_{Xkj} = \max(TX_{Xkj})$	°C
TX_N	Min maximum temperature	Let TX_N be the daily maximum temperature in month k , period j . The minimum daily maximum temperature each month is then: $TX_{Nkj} = \min(TX_{Nkj})$	°C
TN_X	Max minimum temperature	Let TN_X be the daily minimum temperature in month k , period j . The maximum daily minimum temperature each month is then: $TN_{Xkj} = \max(TN_{Xkj})$	°C
TN_N	Min minimum temperature	Let TN_N be the daily minimum temperature in month k , period j . The minimum daily minimum temperature each month is then: $TN_{Nkj} = \min(TN_{Nkj})$	°C
DTR	Diurnal temperature range	Let TN and TX be the daily minimum and maximum temperature respectively on day i in period j . If I represents the number of days in j , then: $DTR_j = \sum_{n=1}^I (TX_{ij} - TN_{ij}) / I$	°C

contains East and central Asia. It has various types of climate zones and a large population, which are extremely vulnerable to extreme climatic disasters. Moreover, the ASA, which is situated east of the Afro-Asian arid zone, is adjacent to the East Asian monsoon area, making it an appropriate place to conduct research on extreme climate change under 1.5 and 2 °C warming targets.

We used the Penman–Monteith formula to calculate PET due to its thorough physical and meteorological processes (Huang *et al.*, 2012; Scheff and Frierson, 2014). For more details on the PET calculation, please refer to Allen *et al.* (1998). Drylands are defined as regions with AI less than 0.65 and are further classified into four subtypes naming hyper-arid ($AI < 0.05$), arid ($0.05 \leq AI < 0.2$), semi-arid ($0.2 \leq AI < 0.5$), and dry sub-humid ($0.5 \leq AI < 0.65$) (Middleton and Thomas, 1997). In our study, we utilized the AI provided by Feng and Fu (2013), which was calculated based a mean state of 1971–2000 that was regarded as the historical period on the basis of the division principle.

2.4 | Statistical methods

For the research findings, box plots and probability distribution functions (PDFs) were used in addition to spatial plots and line charts. Box plots could provide more information about extreme climate indices using 10, 25, 50, 75, and 90% level displays, while the PDFs could describe the data distribution more accurately (Christidis *et al.*, 2005; Alexander and Arblaster, 2009; Fischer *et al.*, 2013; Min *et al.*, 2013; Morak *et al.*, 2013).

Beyond that, two metrics (the probability ratio PR and FAR) were used for attributions, which were defined as $PR = P_1/P_0$ and $FAR = 1 - P_0/P_1$, respectively (Stone and Allen, 2005). P_0 refers to the extreme temperature indices during the historical period, and P_1 represents the same under 1.5 and 2 °C conditions. Both of these metrics could attribute the contributions due to external forcing changes (Pall *et al.*, 2011; Lewis and Karoly, 2013).

3 | RESULTS

3.1 | Spatiotemporal change and detection in threshold indices

Before analysing the extreme temperature indices, it is necessary to estimate the increase in mean temperature over East-central Asia for its climate background effects. According to Figure 1, which illustrates 1.5 °C warming limits (Figure 1a,c,e), 1 pt5 shows an average overall warming distribution, and greater values are situated in southeast China, the Tibetan Plateau, the Iranian Plateau, and the Ural Mountains. Significant differences can be found between 1 pt5 and RCP4.5 (or RCP8.5). Along with the wet–dry boundary (excluding India), the mean temperature increase in most of the ASA

exceed 1.5 °C. Some regions, such as the Ural Mountains in particular, increases even over 2 °C in RCPs, with an average 0.5 °C warmer compared with that of 1 pt5. In contrast, the HA heat up subtly, and most areas vary from 0.5 to 1.5 °C. This indicates the difference between the two methods in terms of reaching the warming targets. For an additional 0.5 °C warming, the condition is completely opposite to the previously situation among different experiments. LWR provide more obvious temperature distributions between the ASA and HA (Figure 1b). Temperature growth in almost all of the ASA regions exceeds 0.5 °C, and in the northwest part it even surpasses 1 °C. Conversely, only a 0.2–0.4 °C slightly increase in the HA is observed, which is less than the global average. The RCP4.5 and RCP8.5 scenarios witness more subtle variations than the LWR, excluding southeast China (Figure 1d,f).

There are two cold indices, as the name suggests, FD stands for the annual number of days when there is conditional frost on the ground, and ID represents the annual number of days when there is conditional ice on the ground. Figure 2 shows that regardless of the scenario, decreasing areas basically exist to the north of 25°N, which is overwhelmingly dominated by the ASA (Figure 2a–f)). It is worth noting that the greatest value would be zonal between 30°N and 40°N. For instance, the middle and lower reaches of the Yangtze River and Tibetan Plateau experience a rapid decrease in all simulation results, whereas the southern areas remain constant due to their temperature rarely being below 0 °C. For the box plots, the ASA median change in FD under the 1.5 °C scenario relative to the historical period would be nearly 10 days/year, which is 2–3 days larger than the HA change (Figure 2g). Likewise, the 2 °C scenario relative to the 1.5 °C scenario would be nearly 5 days/year, which is 2–3 days larger than the HA change (Figure 2h). Nevertheless, because of the contributions of the Yangtze River basin, the amplitude of the HA variation in the 90th interval would be nearly the same as that of the ASA.

Similar to the FD, the spatial distribution of large value regions in ID would also occur in the boreal areas, which most belong to the ASA (Figure 3a–f). Changes in the ID occur further north than those in the FD due to its stricter temperature condition. The Tibetan Plateau and its vicinity would be an interesting region, as it experiences sharp decreases due to its altitude and severe cold. All subplots show that the ID southern boundary would coincide with the wet–dry boundary, that is to say the demarcation line may play an important role in ID change. As for 2 °C relative to 1.5 °C, the amplitude of changes in ID under LWR is larger than that under RCPs. Regardless of the median or 90th interval, the value of the ASA is greater than that of the HA according to the box plots (Figure 3g,h).

Changes in the FD and ID could represent extreme temperature changes during the cold season. Likewise, the SU and TR could represent the same conditions during the warm season. Unlike the latitudinal pattern shown in Figures 2

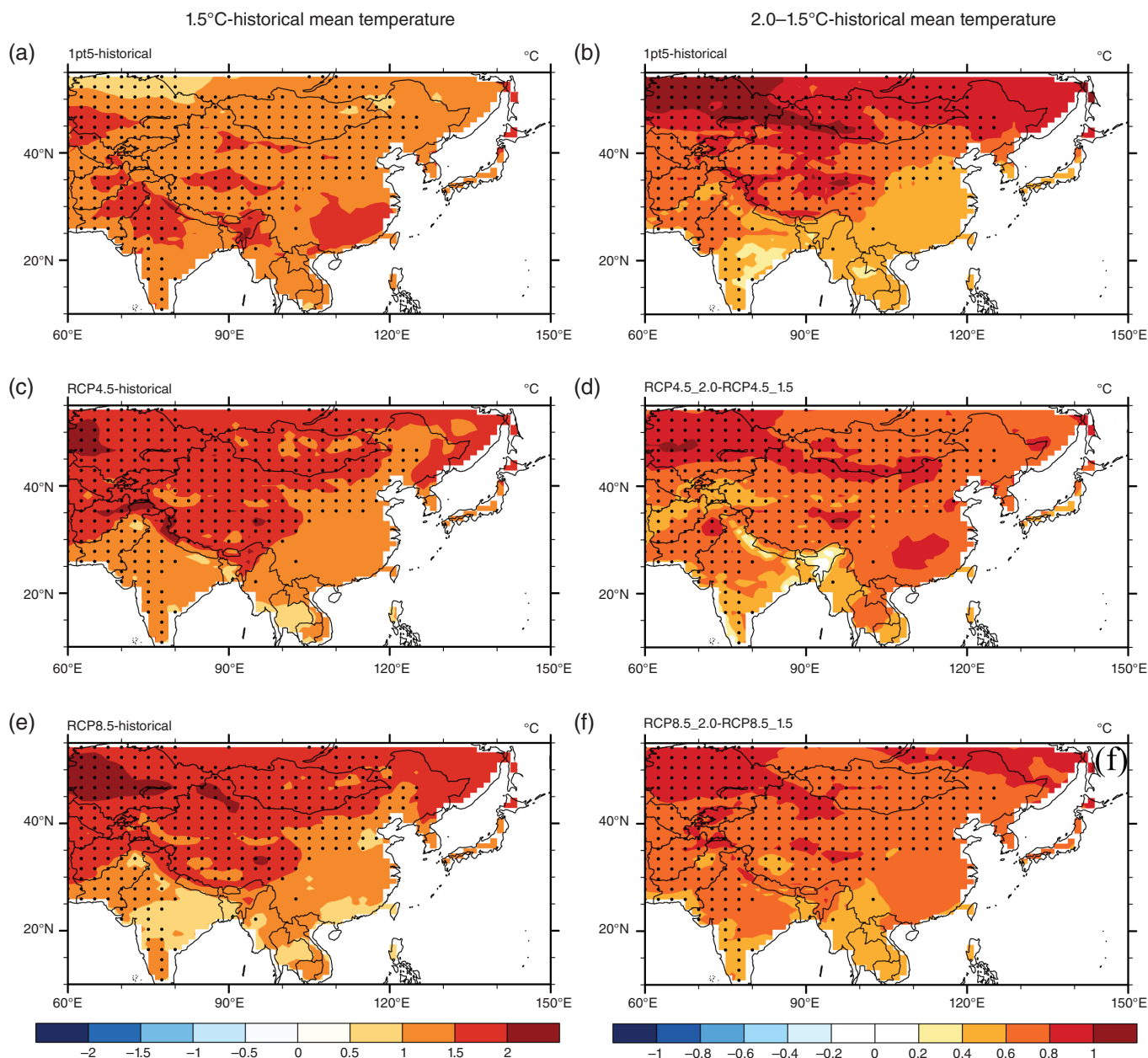


FIGURE 1 Spatial changes in mean temperature in the 1.5 °C scenario relative to the historical period (1971–2000) for (a) 1 pt5, (c) RCP4.5, and (e) RCP8.5. The 2 °C scenario relative to the 1.5 °C scenario for (b) 2 pt, (d) RCP4.5, and (f) RCP8.5. The dotted parts represent ASA [Colour figure can be viewed at wileyonlinelibrary.com]

and 3, a more complex distribution can be found in Figure 4. South Asia and the eastern and central regions of China would experience an increase, in which the HA would comprise a large part. These areas are considered as traditional high-temperature zones. Conversely, the spacious ASA, such as the northern Mongolian Plateau and Tibetan Plateau, would fluctuate slightly, and even a large amount of open space would exist because of the lack of SU days (Figure 4a–f). These discrepancies also reflect those in the box plots. The median changes in the SU in the ASA would be approximately 10 days/year in the 1.5 °C scenario relative to the historical period (Figure 4g) and half in a further 0.5 °C warming world. The increment are almost twice in the HA compared to ASA according to all simulation results (Figure 4h).

Similar to the relationship between the FD and ID, the amplitude of changes in TR increase less than that in SU (Figure 5a–f). Specifically, the growth in north of 50°N (especially in northeast China) would cease and remain steady. Due to the improvement of inclusion index criteria, significant decreases could be found in the box plots. Compared with SU (Figure 4g), the change in TR would sharply decrease by 10 days in HA and 5 days in ASA from the perspective of the median in the box plots (Figure 5g). Likewise, a small increase (less than 5 days) under the additional 0.5 °C warming would take place, but it is not obvious (Figure 5h).

According to the above discussion, we could outline the changes in the selected extreme temperature indices under

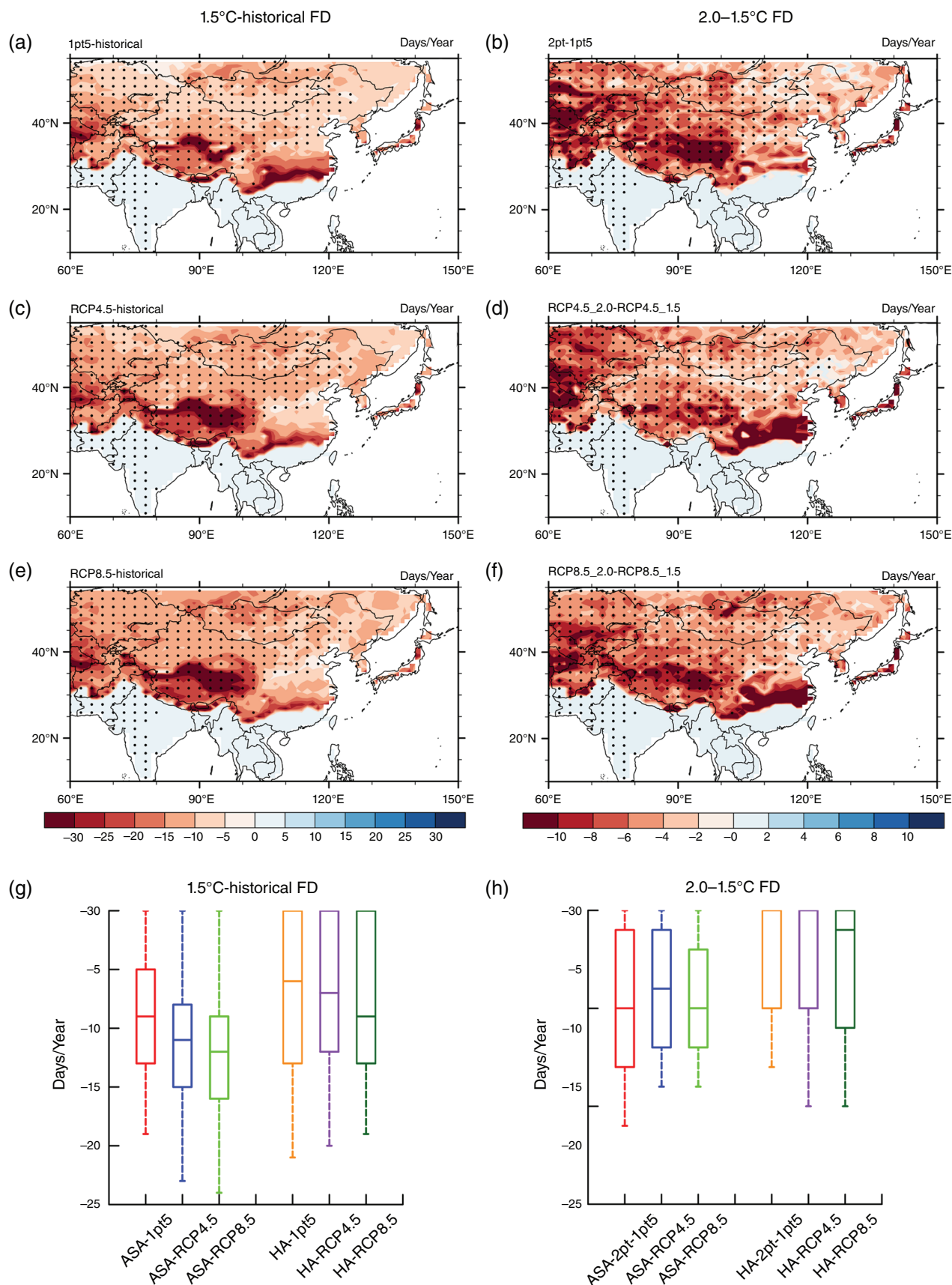


FIGURE 2 Spatial changes in FD in the (a, c, e) 1.5 °C scenario relative to the historical period and (b, d, f) 2 °C scenario relative to the 1.5 °C scenario. For the box plots, subplot (g) refers to the 1.5 °C scenario relative to the historical plots. Subplot (h) refers to the 2 °C scenario relative to the 1.5 °C scenario. The box-whisker plots describe the 10th, 25th, 50th, 75th, and 90th intervals. Red represents LWR in ASA, blue represents the RCP4.5 in ASA, green represents the RCP8.5 in ASA, dark orange represents LWR in HA, purple represents the RCP4.5 in HA, and dark green represents the RCP8.5 in HA [Colour figure can be viewed at wileyonlinelibrary.com]

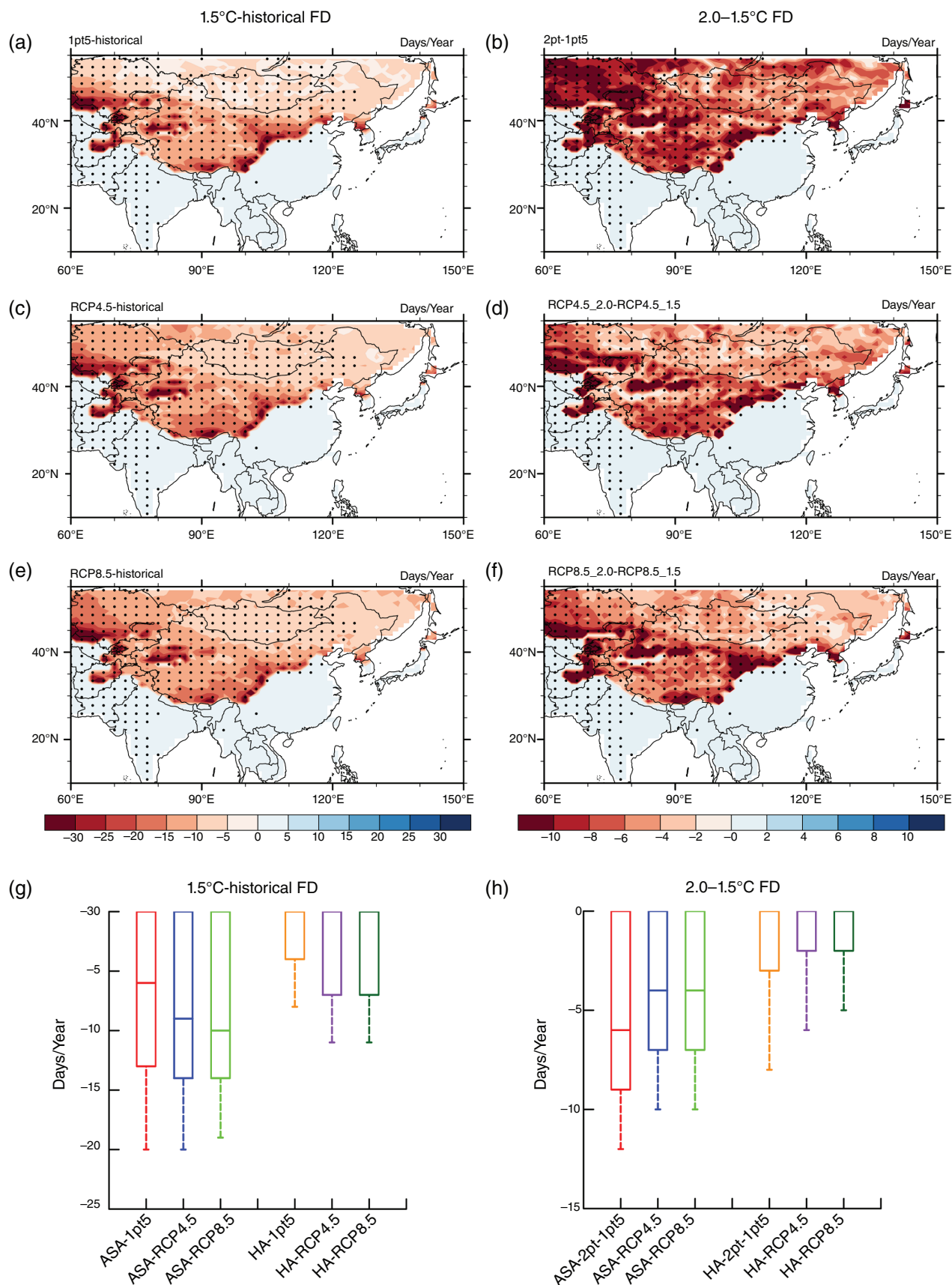


FIGURE 3 Same as Figure 2, but for ID [Colour figure can be viewed at wileyonlinelibrary.com]

1.5 and 2 °C warming targets. For a clearer understanding, temporal variations in the LWR during 1971–2100 are illustrated in Figure 6. The FD shows a steady decrease of

approximately 15% in 2100 compared with the original in both of the ASA and HA (Figure 6a). In addition, there is a large gap in the basic FD days between the ASA and

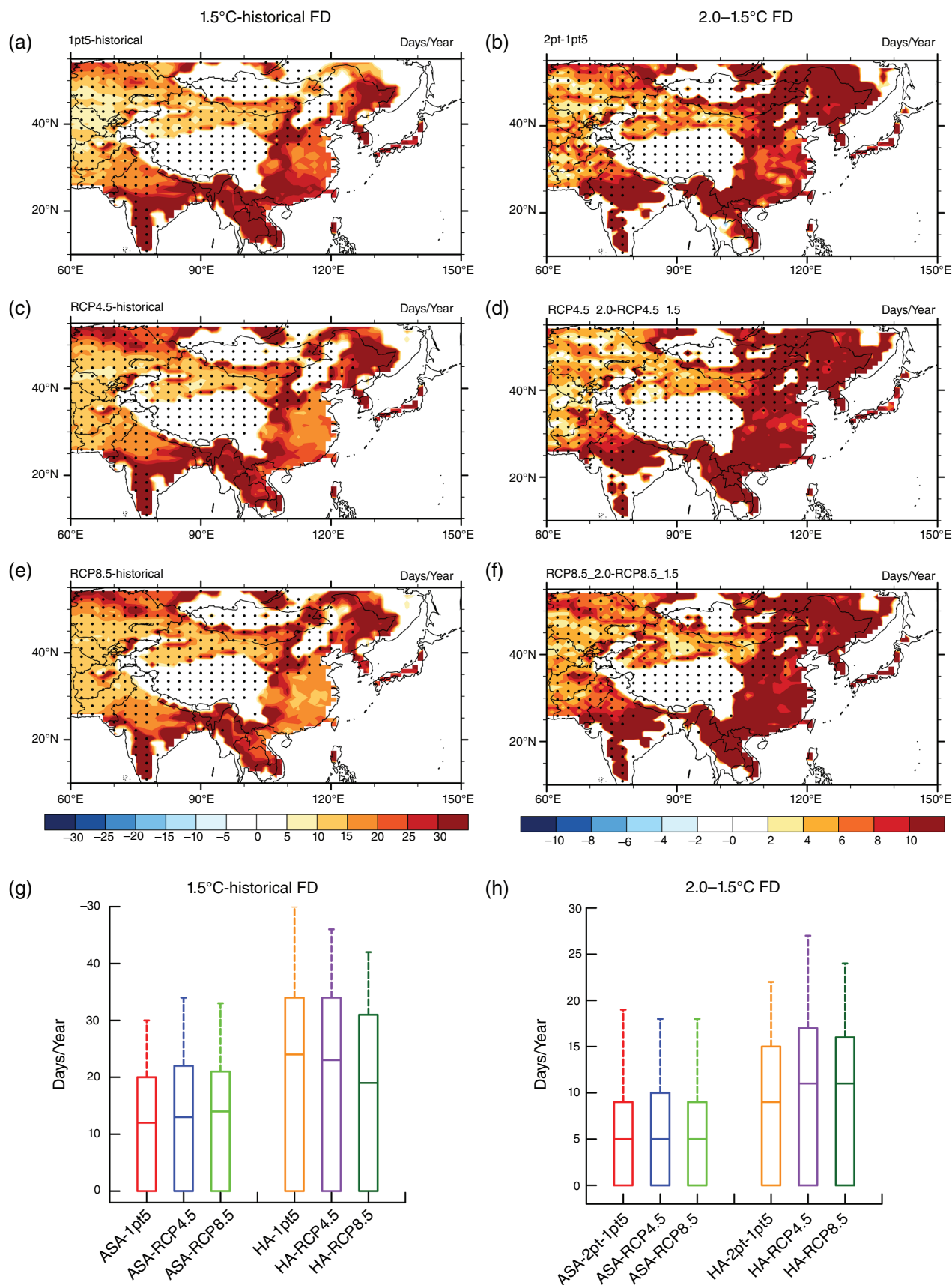


FIGURE 4 Same as Figure 2, but for SU [Colour figure can be viewed at wileyonlinelibrary.com]

HA. The change in ID is similar to that in the FD for most features, and there is only a mere difference in intensity (Figure 6b). The two warm indices reach a peak at

approximately 2040 and then remain stable, the inflection periods are almost the same as those in the cold indices (Figure 6c,d).

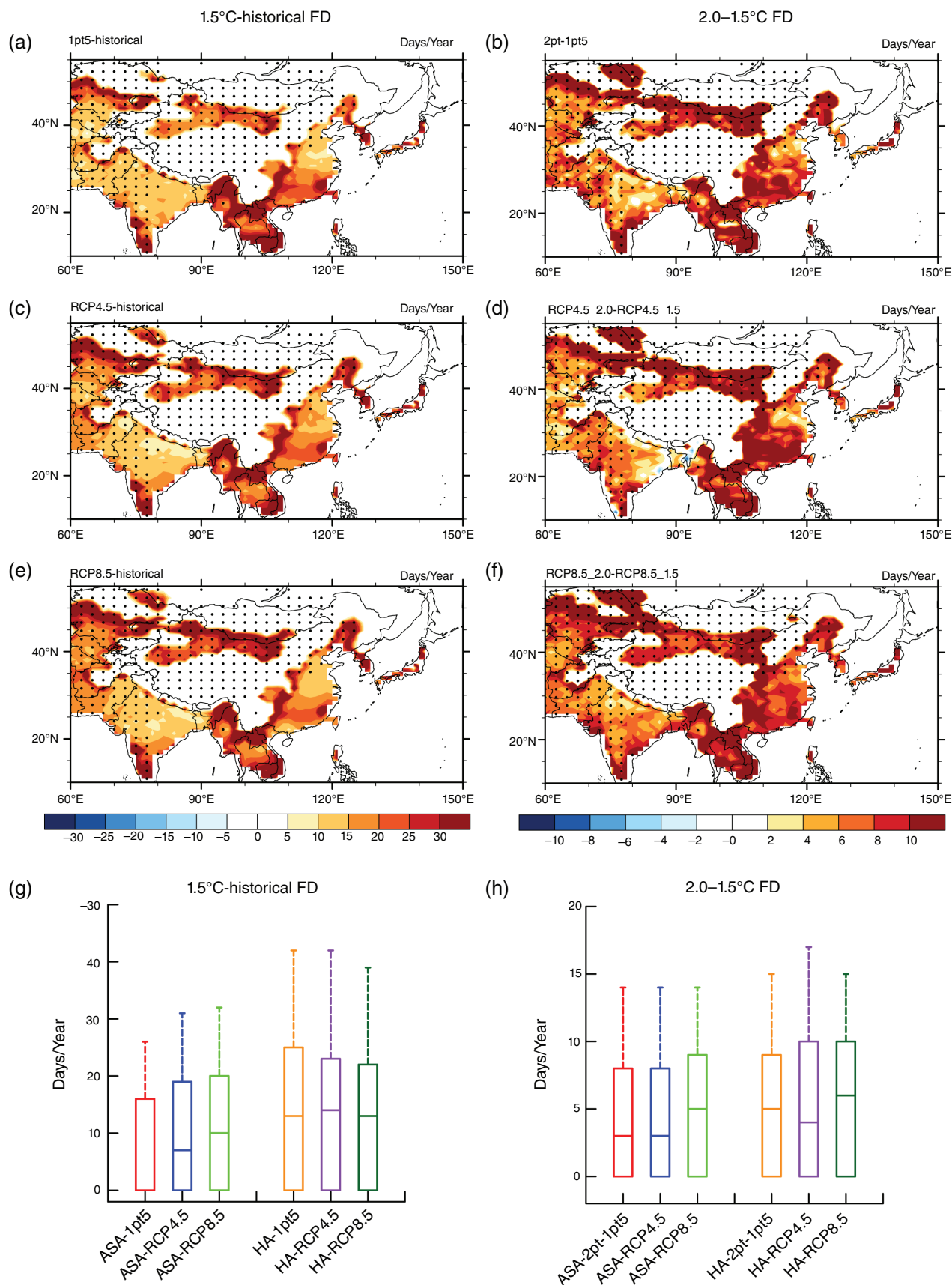


FIGURE 5 Same as Figure 2, but for TR [Colour figure can be viewed at wileyonlinelibrary.com]

Strong correlations between the mean temperature rise and threshold extreme temperature indices can be seen in Figures 2–6. Additionally, attributions and detections are

needed to provide confirmation. We used the FAR and PR to quantify the warming influence on the occurrence of extreme cold or warm temperature indices. As concluded

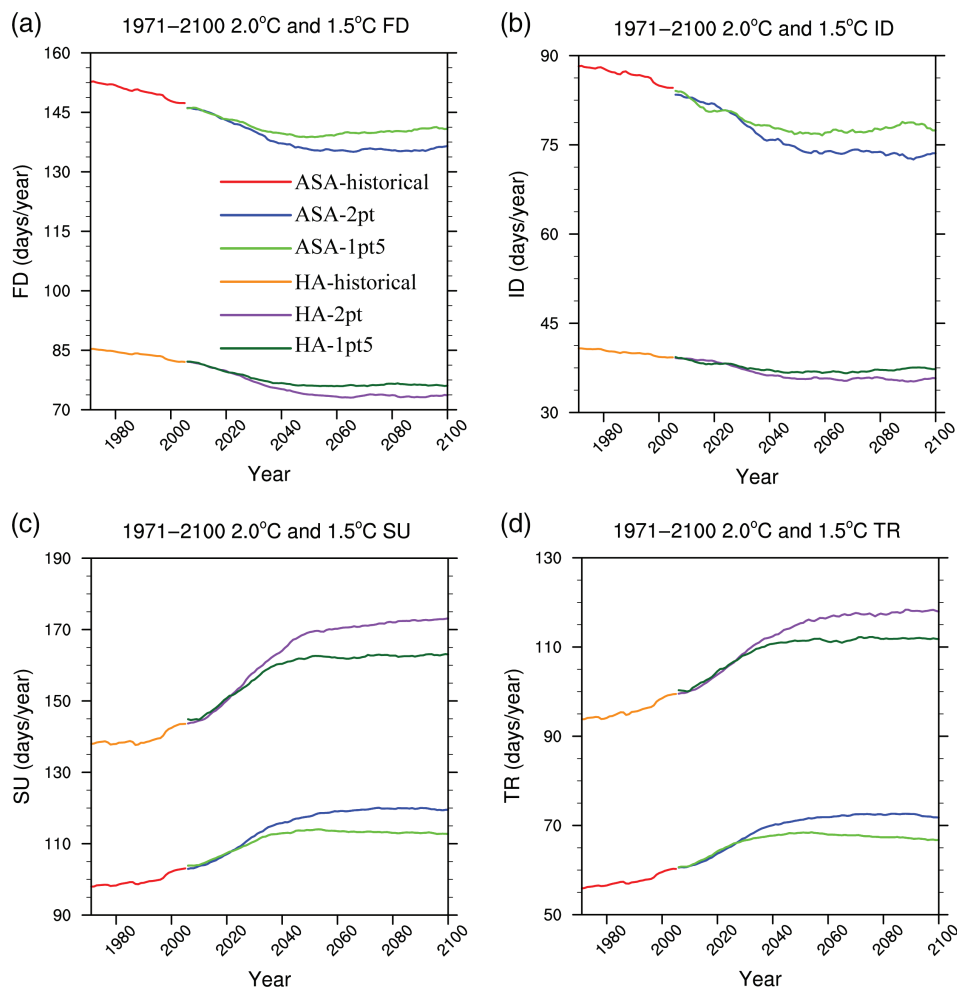


FIGURE 6 Temporal changes during 1971–2100 for (a) FD, (b) ID, (c) SU, and (d) TR. Red lines represent the historical period in ASA, blue lines represent 2 pt in ASA, green lines represent 1 pt5 in ASA, the dark orange lines represent the historical period in HA, purple lines represent 2 pt in HA, and the dark green lines represent 1 pt5 in HA [Colour figure can be viewed at wileyonlinelibrary.com]

before, the increase in mean temperature is negatively related to the cold indices. PR in both the FD and ID decrease by approximately 10% from nearly 1 in 2006 to approximately 0.9 in 2100 (Figure 7a,b). The largest change in FD occurs in the HA and ID in the ASA due to threshold differences. The same descending trend in the FAR indicates that the cold indices occurrence will decrease in the future (Figure 7e,f). Similarity but opposite, the two warm indices reach a plateau and experience a moderate increase (0.15–0.2) (Figure 7c,d,g,h). A warming future exerts a strong influence on extreme temperature indices.

3.2 | PDFs change in absolute indices

To some extent, the threshold extreme climate indices, such as the FD, ID, SU, and TR, refer to the frequency of extreme temperature events, whereas TX_X , TX_N , TN_X , TN_N could indicate the intensities (Alexander *et al.*, 2006). For a scenario of 1.5 °C warming relative to the historical period, TX_X in winter would have the largest amplitude and peaks at 1.5–1.8 °C in December. The ASA are projected to experience a greater temperature increase in summer which is

approximately 0.2–0.3 °C on average higher than that of the HA. The remaining three seasons are not show obvious discrepancies, and the gaps between the ASA and HA are narrower than those in summer. However, it is a different situation when a 0.5 °C change occurs. Almost all experiments exceed 0.5 °C in the whole year (figures not shown). The PDFs graph could show an all-sided perspective about the temperature ranges, which contain more climatic change information (Christidis *et al.*, 2011; Fischer and Knutti, 2014). In general, ASA experiments reach a higher point than the HA experiments, and the median number are equivalent to 1.5 °C in the two 1.5 °C scenarios relative to the historical scenario (Figure 8a,i). Conversely, both additional 0.5 °C scenarios portray moderately different graphs in the average TX_X , which are approximately 0.2 °C higher than the 0.5 °C global mean rise (Figure 8e,m). In addition, the TX_X increase in winter is higher than that in summer. TX_N is similar to TX_X in the form of concrete data variations, with a less than average value under 1.5 °C warming limits and a greater than average value under 2.0 °C warming limits. Therefore, changes in the maximum temperature might have the same patterns. Likewise, the consistency of

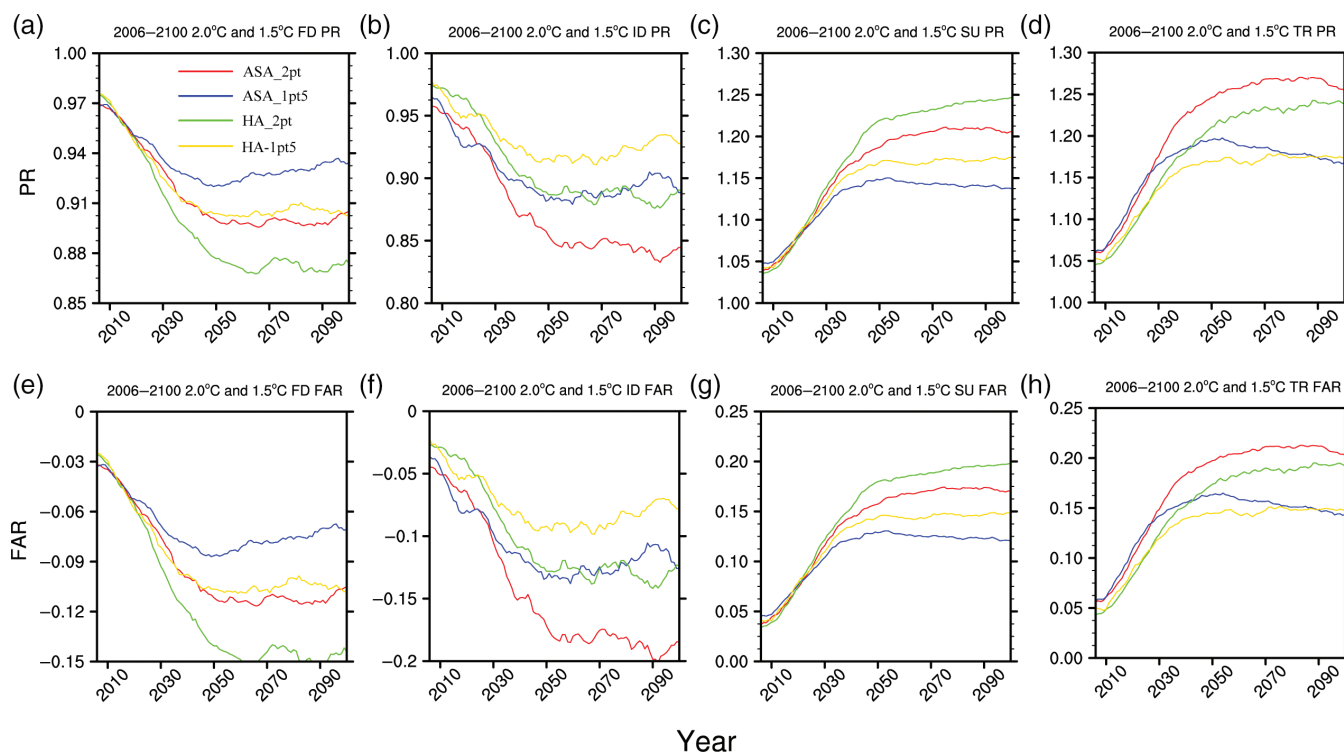


FIGURE 7 (a, e) FD, (b, f) ID, (c, g) SU, (d, h) TR PR and FAR values for the 2 °C scenario and the 1.5 °C scenario relative to the historical period in both ASA and HA. The red line represents the 2 °C scenario in ASA, the blue line represents the 1.5 °C scenario in ASA, the green line represents the 2 °C scenario in HA, and the gold line represents the 1.5 °C scenario in HA [Colour figure can be viewed at wileyonlinelibrary.com]

the PDFs in the TX_N is as good as that of the monthly changes. All four figures (Figure 8b,f,j,n) provide similar distributions. The ASA experiments are slightly larger than the HA experiments. The PDFs distribution forms are basically the same as those of the TX_X . Figure 8c shows the difference in TN_X between the ASA and HA, with median values of approximately 1.2 °C (HA) and 1.7 °C (ASA). The right-tail distribution of the PDFs in TN_X in Figure 8k exceeds 3.0 °C, and it is the largest value of the four indices under 1.5 °C warming target. However, there is not a large change in the average value. As for 2 °C relative to 1.5 °C in summer, the increasing rate in TN_X returns to normal (Figure 8g). In comparison, TN_X has a small advantage in winter conditions compared to summer (Figure 8o). Recent studies have indicated that the minimum temperature has a higher increase rate than the maximum temperature, especially in the mid- and high-latitude areas in the Northern Hemisphere (Huang *et al.*, 2012; Guan *et al.*, 2015). Figure 8p could partly support this conclusion. The extreme value reaches approximately 2–2.5 °C in some vulnerable areas with an additional 0.5 °C in winter. In summary, the rapid increase in extreme temperature, especially the minimum temperature, is of great concern.

3.3 | Spatiotemporal change in DTR

The DTR could show the relative changes in the maximum temperature and the minimum temperature under future climate change. Besides, it is vital for flora and fauna health.

For instance, high temperatures during the daytime are conducive to producing organic matter by vegetation photosynthesis, and low temperatures at night could reduce the respiratory loss of vegetation and increase the accumulation rate of organic matter (Atkin *et al.*, 2000). Therefore, in general, the larger the DTR is, the more conducive to the growth and development of vegetation. In Figures 9 and 10, the DTR represents summer and winter mean differences rather than monthly mean differences between the maximum temperature and the minimum temperature. There are large positive regions in northern India and the Tibetan Plateau and an extension of the Loess Plateau in the northeast plain in 1 pt5 relative to the historical period (Figure 9a). These regions are also obvious in the three additional 0.5 °C conditions. The DTR in the northern Mongolian Plateau shows a stable steadiness or a slight decrease (Figure 9b,d,f). However, the entire research areas experience a slight decrease under 1.5 °C warming limits in RCP4.5 and RCP8.5 (Figure 9c,e). The distributions are completely different in Figure 10. All subplots witness a tremendous gap along the ASA and HA transition zone. The DTR drops in most of the ASA and increases in most of the HA, especially in southeast China. The increase is up to approximately 0.6–1.0 °C in the 1.5 °C scenarios relative to the historical period (Figure 10a–c) in the HA. For the additional 0.5 °C warming, there is a 0.3–0.6 °C increase (Figure 10d–f). Moreover, an average decrease of 0.3–0.6 °C could be found in the ASA. Given additional research, the maximum temperature contributes more in summer, and the minimum temperature is the

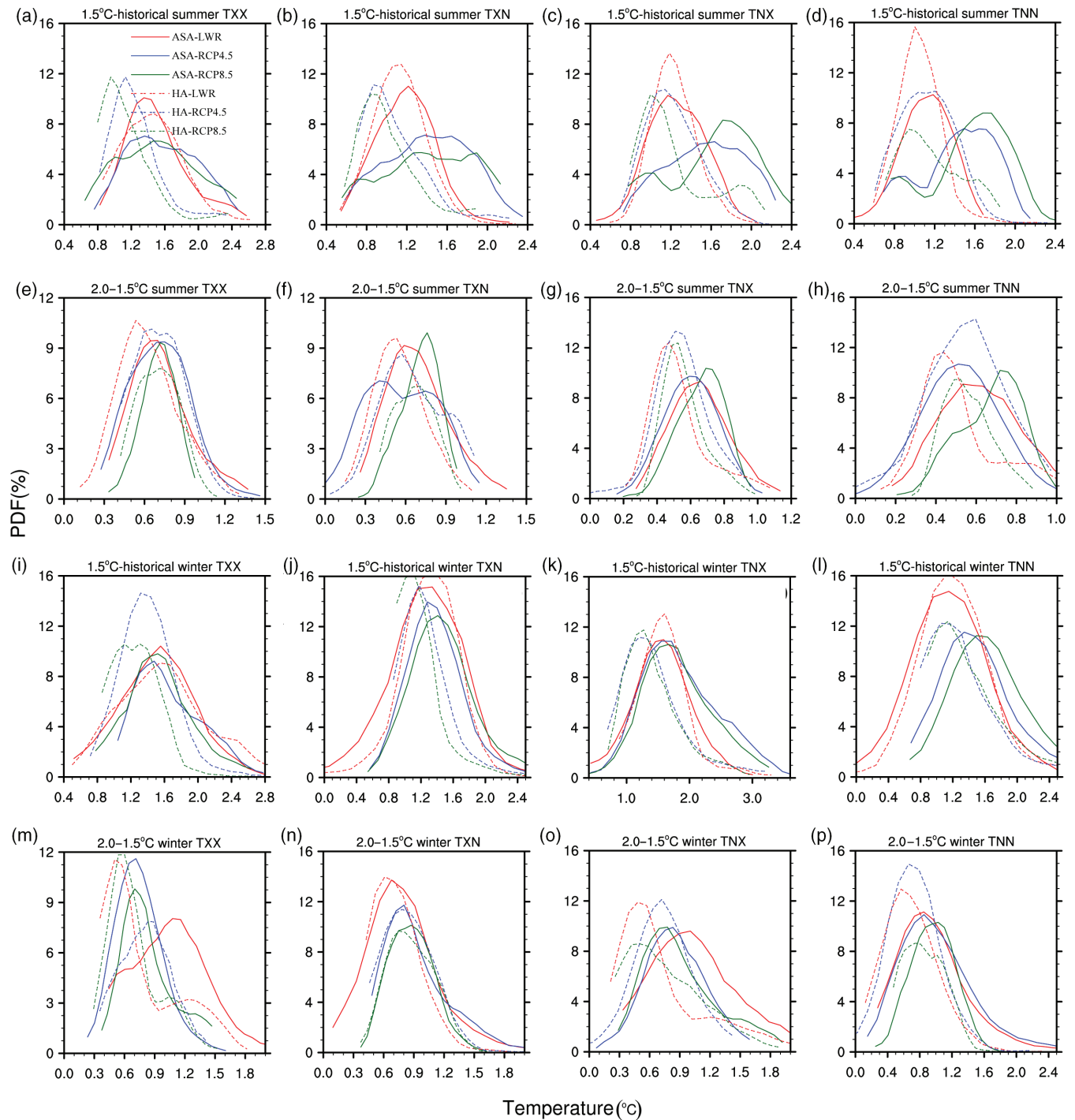


FIGURE 8 Temperature PDFs distribution about (a, e, i, m) TX_X , (b, f, j, n) TX_N , (c, g, k, o) TN_X , and (d, h, l, p) TN_N in both summer and winter under the 1.5 °C scenario relative to the historical period and the 2 °C scenario relative to the 1.5 °C scenario. The solid red line represents LWR in ASA, the solid blue line represents RCP4.5 in ASA, the solid green line represents RCP8.5 in ASA, the dashed red line represents LWR in humid areas HA, the dashed blue line represents RCP4.5 in HA, and the dashed green line represents RCP8.5 in HA [Colour figure can be viewed at wileyonlinelibrary.com]

dominant factor in winter (figures not shown). The most likely reason is that in summer, the decrease of cloud amount in the warming future reflect less solar radiation and cause more positive effect in the maximum temperature than the minimum temperature in dry–wet transition zone, thus leads to an increase in DTR. As for winter, the correlation between cloud amount and DTR is weaker than that in summer (Liu *et al.*, 2018). For most East–central Asia regions, the increase in the minimum temperature results in the

decrease in DTR. However, the maximum temperature is the dominant factor in southeast China. And in those regions, DTR shows an increase.

4 | DISCUSSION AND CONCLUSION

We used CESM short-term stabilization response representative LWR and transient climate response representative

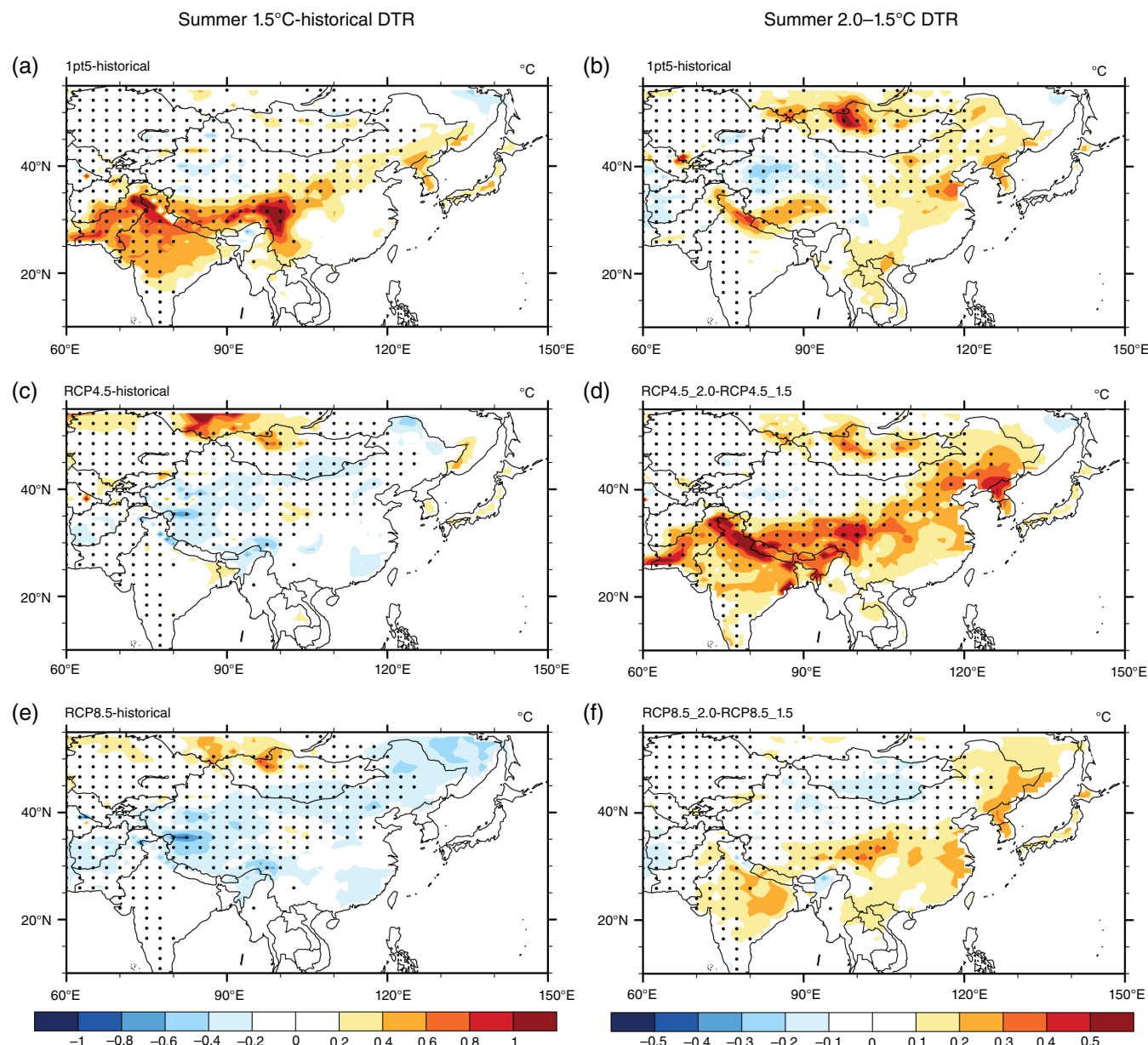


FIGURE 9 Spatial changes of the DTR in the 1.5 °C scenario relative to historical (1971–2000) for (a) 1 pt5, (c) RCP4.5, and (e) RCP8.5. 2 °C scenario relative to 1.5 °C scenario for (b) 2 pt, (d) RCP4.5, and (f) RCP8.5. The dotted parts represent the ASA [Colour figure can be viewed at wileyonlinelibrary.com]

RCP4.5 and RCP8.5 to analyse the spatiotemporal variations over East and central Asia. Similar to the previous study, we find that the warm extreme indices increase significantly due to 0.5 °C additional warming, whereas cold extreme indices show remarkable decrease (Schleussner *et al.*, 2016; Wang *et al.*, 2017). The trends of potential risks (FAR and PR) indicate that the warmer the world is, the more frequency the climate extreme events are projected to occur. Although limited samples in CESM model were utilized in our research, the variation of temperature extremes under different warming conditions are illustrated clearly. Here are some specific conclusions:

Compared with the historical period, the mean temperature increase over East and central Asia generally exceed the global average. In addition, a further 0.5 °C warming results

in a mean temperature rise of 0.6–1 °C. Due to the remarkable temperature increase in central Asia, our result is slightly larger than that mentioned by Li *et al.* (2018a), which are about 1.7 and 2.3 °C above pre-industrial levels in the 1.5 and 2 °C warming limits, respectively. The two indices representing the cold season (FD and ID) experience a moderate decrease in the ASA and dry–wet dividing zone, especially in the Tibetan Plateau. There are an approximate 5 days/year decline in both the ASA and HA due to an additional 0.5 °C warming. For warm indices, a large change in the SU occurs in the HA such as East China, Southeast Asia, and South India, which is 20 days/year larger in the 1.5 °C scenario relative to the historical period and 10 days/year larger under additional 0.5 °C warming from 1.5 to 2 °C. The trend in the TR is similar to that in the SU, but under more

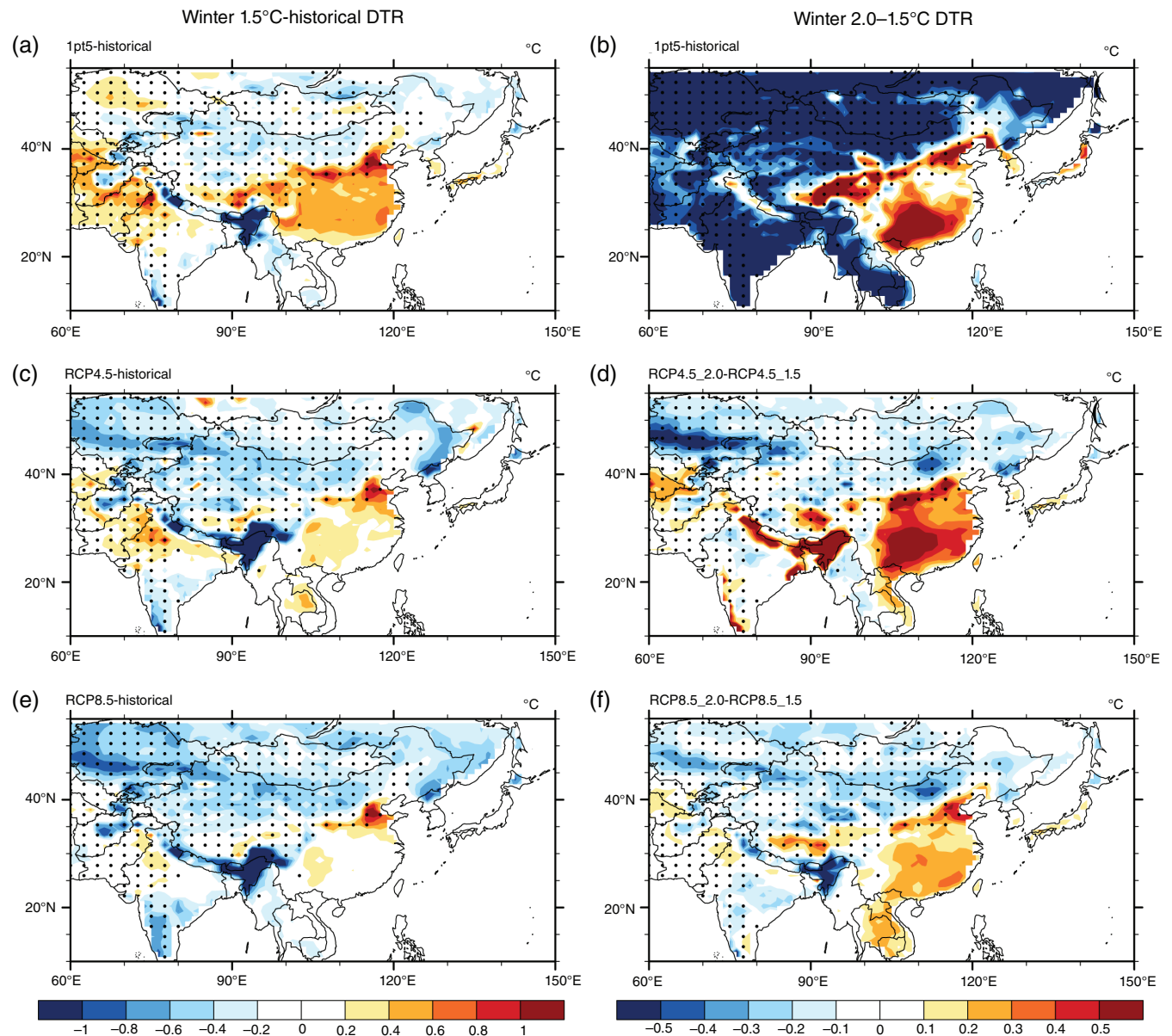


FIGURE 10 Same as Figure 9, but for winter [Colour figure can be viewed at wileyonlinelibrary.com]

demanding conditions, the variations are smaller both temporally and spatially. Sui *et al.* (2018) pointed out that the occurrence of SU and TR last almost the entire summer in China under 2 °C warming limits. More than 6 and 11% of the increases in SU and TR could be reduced if we limit global warming to 1.5 °C (Li *et al.*, 2018b). Moreover, East Asia would avoid about 20% severe heat stress compared with 2 °C target (Lee and Min, 2018).

Four significant features are found in four intensity indices (TX_X , TX_N , TN_X , and TN_N), with variations under the 1.5 and 2 °C warming targets. (a) The increasing range for the minimum temperature is slightly greater than that for the maximum temperature, especially under an additional 0.5 °C warming. (b) The indices in winter is 0.2–0.4 °C larger than those in summer. (c) As a whole, there are no obvious differences between the ASA and HA. (d) The growth trend of these selected indices is nonlinear; an additional 0.5 °C

warming will make a large difference in extreme temperature increases. Li *et al.* (2018a) also supported that the 0.5 °C less warming in the 1.5 °C warming limits over East Asia help avoid about 35% impacts in TX_X and TN_X .

The DTR is projected to experience a 0.3–0.5 °C increase in and near the dry–wet transition zone in summer under the condition of a 0.5 °C warmer world. However, positive values in East and central China and negative values in other parts of East–central Asia lead to a huge difference in winter. Previous studies indicated that the DTR shows a significantly decreasing trend at historical period over most of the globe, including East–central Asia (Liu *et al.*, 2018). This phenomenon could be attributed for the minimum temperature increased more rapidly than the maximum temperature (Vose *et al.*, 2005). Different from the homogenous decrease trend at historical period, we found the DTR in some subregions increase while in the other subregions

decrease under 1.5 or 2 °C warming future. And it still have strong associate with the cloud cover.

Therefore, limiting global warming to 1.5 °C is benefit for us humans in terms of reducing climate extremes in intensity, frequency, and duration over East-central Asia. We hope these research achievements could offer necessary help for policy makers. However, more global and regional climate models and more 1.5 and 2 °C warming experiment samples should be included to better understand the changes in climate extremes in further study.

ACKNOWLEDGEMENTS

This work was jointly supported by the National Natural Science Foundation of China (41705077 and 41630426), China Postdoctoral Science Foundation (2017M613250), and the National Key Research and Development Program of China (2017YFC1502305). The authors acknowledge the NCAR for releasing the CESM low-warming experiment products and the data were acquired from <http://www.cesm.ucar.edu/experiments/1.5-2.0-targets.html>.

ORCID

Meng Zhang  <https://orcid.org/0000-0003-3643-9501>

Yun Wei  <https://orcid.org/0000-0002-2965-1881>

REFERENCES

- AghaKouchak, A., Cheng, L.Y., Mazdiyasni, O. and Farahmand, A. (2014) Global warming and changes in risk of concurrent climate extremes: insights from the 2014 California drought. *Geophysical Research Letters*, 41(24), 8847–8852. <https://doi.org/10.1002/2014GL062308>.
- Alexander, L.V. and Arblaster, J.M. (2009) Assessing trends in observed and modelled climate extremes over Australia in relation to future projections. *International Journal of Climatology*, 29(3), 417–435. <https://doi.org/10.1002/joc.1730>.
- Alexander, L. V., Zhang, X., Peterson, T. C., Caesar, J., Gleason, B., Tank, A., Haylock, M., Collins, D., Trewin, B., Rahimzadeh, F., Tagipour, A., Kumar, K., Revadekar, J., Griffiths, G., Vincent, L., Stephenson, D. B., Burn, J., Aguilar, E., Brunet, M., Taylor, M., New, M., Zhai, P., Rusticucci, M. and Vazquez-Aguirre, J. L. (2006) Global observed changes in daily climate extremes of temperature and precipitation. *Journal of Geophysical Research: Atmospheres*, 111(D5), D05109. <https://doi.org/10.1029/2005JD006290>.
- Allen, R.G., Pereira, L.S., Raes, D. and Smith, M. (1998) *Crop Evapotranspiration: Guidelines for Computing Crop Water Requirements*. FAO Irrigation and Drainage Paper 56. Rome: FAO.
- Atkin, O.K., Holly, C. and Ball, M.C. (2000) Acclimation of snow gum (*Eucalyptus pauciflora*) leaf respiration to seasonal and diurnal variations in temperature: the importance of changes in the capacity and temperature sensitivity of respiration. *Plant, Cell, & Environment*, 23(1), 15–26. <https://doi.org/10.1046/j.1365-3040.2000.00511.x>.
- Barriopedro, D., Fischer, E.M., Luterbacher, J., Trigo, R. and Garcia-Herrera, R. (2011) The hot summer of 2010: redrawing the temperature record map of Europe. *Science*, 332(6026), 220–224. <https://doi.org/10.1126/science.1201224>.
- Cattiaux, J., Vautard, R., Cassou, C., Yiou, P., Masson-Delmotte, V. and Codron, F. (2010) Winter 2010 in Europe: a cold extreme in a warming climate. *Geophysical Research Letters*, 37, L20704. <https://doi.org/10.1029/2010GL044613>.
- Chen, H.P. and Sun, J.Q. (2014) Changes in climate extreme events in China associated with warming. *International Journal of Climatology*, 35(10), 2735–2751. <https://doi.org/10.1002/joc.4168>.
- Chen, H.P. and Sun, J.Q. (2015) Changes in drought characteristics over China using the standardized precipitation evapotranspiration index. *Journal of Climate*, 28(13), 5430–5447. <https://doi.org/10.1175/JCLI-D-14-00707.1>.
- Chen, H.P. and Sun, J.Q. (2018) Projected changes in climate extremes in China in a 1.5 °C warmer world. *International Journal of Climatology*, 38(9), 3607–3617. <https://doi.org/10.1002/joc.5521>.
- Chen, X. Y., Zhang, X. B., Church, J. A., Watson, C. S., King, M. A., Monselesan, D., Legresy, B. and Harig, C. (2017) The increasing rate of global mean sea-level rise during 1993–2014. *Nature Climate Change*, 7(7), 492–495. <https://doi.org/10.1038/NCLIMATE3325>.
- Christidis, N., Stott, P.A., Brown, S., Hegerl, G.C. and Caesar, J. (2005) Detection of changes in temperature extremes during the second half of the 20th century. *Geophysical Research Letters*, 32(20), L20716. <https://doi.org/10.1029/2005GL023885>.
- Christidis, N., Stott, P.A. and Brown, S. (2011) The role of human activity in the recent warming of extremely warm daytime temperatures. *Journal of Climate*, 24(7), 1922–1930. <https://doi.org/10.1175/2011JCLI1510.1>.
- Coumou, D. and Rahmstorf, S. (2012) A decade of weather extremes. *Nature Climate Change*, 2(7), 491–496. <https://doi.org/10.1038/NCLIMATE1452>.
- DeMott, P.J., Sassen, K., Poellot, M.R., Baumgardner, D., Rogers, D.C., Brooks, S.D., Prenni, A.J. and Kreidenweis, S.M. (2003) African dust aerosols as atmospheric ice nuclei. *Geophysical Research Letters*, 30(14), 1732. <https://doi.org/10.1029/2003GL017410>.
- Dole, R., Hoerling, M., Perlwitz, J., Eischeid, J., Pegion, P., Zhang, T., Quan, X. W., Xu, T. and Murray, D. (2011) Was there a basis for anticipating the 2010 Russian heat wave? *Geophysical Research Letters*, 38, L06702. <https://doi.org/10.1029/2010GL046582>.
- Donat, M.G., Alexander, L.V., Yang, H., Durre, I., Vose, R., Dunn, R.J.H., Willett, K.M., Aguilar, E., Brunet, M., Caesar, J., Hewitson, B., Jack, C., Klein Tank, A.M.G., Kruger, A.C., Marengo, J., Peterson, T.C., Renom, M., Oria Rojas, C., Rusticucci, M., Salinger, J., Elrayah, A.S., Sekele, S.S., Srivastava, A.K., Trewin, B., Villarroel, C., Vincent, L.A., Zhai, P., Zhang, X. and Kitching, S. (2013) Updated analyses of temperature and precipitation extreme indices since the beginning of the twentieth century: the HadEX2 dataset. *Journal of Geophysical Research: Atmospheres*, 118(5), 2098–2118. <https://doi.org/10.1002/jgrd.50150>.
- Dosio, A. and Fischer, E.M. (2018) Will half a degree make a difference robust projections of indices of mean and extreme climate in Europe under 1.5 °C, 2 °C, and 3 °C global warming. *Geophysical Research Letters*, 45(2), 935–944. <https://doi.org/10.1002/2017GL076222>.
- Evan, A.T., Vimont, D.J., Heidinger, A.K., Kossin, J.P. and Bennartz, R. (2009) The role of aerosols in the evolution of tropical North Atlantic Ocean temperature anomalies. *Science*, 324(5928), 778–781. <https://doi.org/10.1126/science.1167404>.
- Feng, S. and Fu, Q. (2013) Expansion of global drylands under a warming climate. *Atmospheric Chemistry and Physics*, 13(19), 10081–10094. <https://doi.org/10.5194/acp-13-10081-2013>.
- Fischer, E.M. and Knutti, R. (2014) Detection of spatially aggregated changes in temperature and precipitation extremes. *Geophysical Research Letters*, 41(2), 547–554. <https://doi.org/10.1002/2013GL058499>.
- Fischer, E.M., Beyerle, U. and Knutti, R. (2013) Robust spatially aggregated projections of climate extremes. *Nature Climate Change*, 3(12), 1033–1038. <https://doi.org/10.1038/NCLIMATE2051>.
- Fu, Q. and Feng, S. (2013) Responses of terrestrial aridity to global warming. *Journal of Geophysical Research: Atmospheres*, 119, 7863–7875. <https://doi.org/10.1002/2014JD021608>.
- Guan, X.D., Huang, J.P., Guo, R.X., Yu, H.P., Lin, P. and Zhang, Y.T. (2015) Role of radiatively forced temperature changes in enhanced semi-arid warming in the cold season over East Asia. *Atmospheric Chemistry and Physics*, 15(23), 13777–13786. <https://doi.org/10.5194/acp-15-13777-2015>.
- Guiot, J. and Cramer, W. (2015) Climate change: the 2015 Paris Agreement thresholds and Mediterranean basin ecosystems. *Science*, 354(6311), 465–468. <https://doi.org/10.1126/science.aah5015>.
- Guo, L., Wang, K.C. and Bluestein, H.B. (2016) Variability of tornado occurrence over the continental United States since 1950. *Journal of Geophysical Research: Atmospheres*, 121(12), 6943–6953. <https://doi.org/10.1002/2015JD024465>.
- van Hooijdonk, R., Maynard, J., Tamelander, J., Gove, J., Ahmadi, G., Raymundo, L., Williams, G., Heron, S.F. and Planes, S. (2016) Local-scale projections of coral reef futures and implications of the Paris Agreement. *Scientific Reports*, 6, 39666. <https://doi.org/10.1038/srep39666>.

- Huang, J.P., Guan, X.D. and Ji, F. (2012) Enhanced cold-season warming in semi-arid regions. *Atmospheric Chemistry and Physics*, 12(12), 5391–5398. <https://doi.org/10.5194/acp-12-5391-2012>.
- Huang, J.P., Yu, H.P., Guan, X.D., Wang, G.Y. and Guo, R.X. (2016a) Accelerated dryland expansion under climate change. *Nature Climate Change*, 6(2), 166. <https://doi.org/10.1038/NCLIMATE2837>.
- Huang, J.P., Ji, M.X., Xie, Y.K., Wang, S.S., He, Y.L. and Ran, J.J. (2016b) Global semi-arid climate change over last 60 years. *Climate Dynamics*, 46 (3–4), 1131–1150. <https://doi.org/10.1007/s00382-015-2636-8>.
- Huang, J.P., Yu, H.P., Dai, A.G., Wei, Y. and Kang, L.T. (2017a) Drylands face potential threat under 2 °C global warming target. *Nature Climate Change*, 7 (6), 417–422. <https://doi.org/10.1038/NCLIMATE3275>.
- Huang, J. P., Li, Y., Fu, C. B., Chen, F. H., Fu, Q., Dai, A. G., Shinoda, M., Ma, Z. G., Guo, W., Li, Z., Zhang, L., Liu, Y. Z., Yu, H. P., He, Y. L., Xie, Y. K., Guan, X. D., Ji, M. X., Lin, L., Wang, S. S., Yan, H. R. and Wang, G. Y. (2017b) Dryland climate change: recent progress and challenges. *Reviews of Geophysics*, 55(3), 719–778. <https://doi.org/10.1002/2016RG000550>.
- James, R., Washington, R., Schleussner, C.F., Rogelj, J. and Conway, D. (2017) Characterizing half-a-degree difference: a review of methods for identifying regional climate responses to global warming targets. *WIREs: Climate Change*, 8(2), e457. <https://doi.org/10.1002/wcc.457>.
- King, A.D., Karoly, D.J. and Henley, B.J. (2017) Australian climate extremes at 1.5 °C and 2 °C of global warming. *Nature Climate Change*, 7(6), 412–416. <https://doi.org/10.1038/NCLIMATE3296>.
- King, A.D., Donat, M.G., Lewis, S.C., Henley, B.J., Mitchell, D.M., Stott, P.A., Fischer, E.M. and Karoly, D.J. (2018) Reduced heat exposure by limiting global warming to 1.5 °C. *Nature Climate Change*, 8(7), 549–551. <https://doi.org/10.1038/s41558-018-0191-0>.
- Kraaijenbrink, P.D.A., Bierkens, M.F.P., Lutz, A.F. and Immerzeel, W.W. (2017) Impact of a global temperature rise of 1.5 °C on Asia's glaciers. *Nature*, 549(7671), 257–260. <https://doi.org/10.1038/nature23878>.
- Lee, S.M. and Min, S.K. (2018) Heat stress changes over East Asia under 1.5 °C and 2.0 °C global warming targets. *Journal of Climate*, 31(7), 2819–2831. <https://doi.org/10.1175/JCLI-D-17-0449.1>.
- Lewis, S.C. and Karoly, D.J. (2013) Anthropogenic contributions to Australia's record summer temperatures of 2013. *Geophysical Research Letters*, 40(14), 3705–3709. <https://doi.org/10.1002/grl.50673>.
- Li, Q., Zhang, R.H. and Wang, Y. (2016) Interannual variation of the wintertime fog-haze days across central and eastern China and its relation with East Asian winter monsoon. *International Journal of Climatology*, 36(1), 346–354. <https://doi.org/10.1002/joc.4350>.
- Li, H.X., Chen, H.P., Wang, H.J. and Yu, E.T. (2018) Future precipitation changes over China under 1.5 °C and 2.0 °C global warming targets by using CORDEX regional climate models. *Science of the Total Environment*, 640, 543–554. <https://doi.org/10.1016/j.scitotenv.2018.05.324>.
- Li, D.H., Zhou, T.J., Zou, L.W., Zhang, W.X. and Zhang, L.X. (2018a) Extreme high-temperature events over East Asia in 1.5 °C and 2 °C warmer futures: analysis of NCAR CESM low-warming experiments. *Geophysical Research Letters*, 45(3), 1541–1550. <https://doi.org/10.1002/2017GL076753>.
- Li, D.H., Zou, L.W. and Zhou, T.J. (2018b) Extreme climate event changes in China in the 1.5 °C and 2 °C warmer climates: results from statistical and dynamical downscaling. *Journal of Geophysical Research: Atmospheres*, 123(18), 10196–10211. <https://doi.org/10.1029/2018JD028835>.
- Lin, L., Wang, Z.L., Xu, Y.Y., Zhang, X.Y., Zhang, H. and Dong, W.J. (2018) Additional intensification of seasonal heat and flooding extreme over China in a 2 °C warmer world compared to 1.5 °C. *Earth's Future*, 6(7), 968–978. <https://doi.org/10.1029/2018EF000862>.
- Liu, L., Guo, J., Chen, W., Wu, R., Wang, L., Gong, H., Xue, W. and Li, J. (2018) Large-scale pattern of the diurnal temperature range changes over East Asia and Australia in boreal winter: a perspective of atmospheric circulation. *Journal of Climate*, 31(7), 2715–2728. <https://doi.org/10.1175/JCLI-D-17-0608.1>.
- Middleton, N.J. and Thomas, D.S.G. (1992) *UNEP: World Atlas of Desertification*. Sevenoaks: Edward Arnold.
- Middleton, N.J. and Thomas, D.S.G. (1997) *World Atlas of Desertification*, 2nd edition. London: Arnold.
- Min, S.K., Zhang, X.B., Zwiers, F., Shiogama, H., Tung, Y.S. and Wehner, M. (2013) Multimodel detection and attribution of extreme temperature changes. *Journal of Climate*, 26(19), 7430–7451. <https://doi.org/10.1175/JCLI-D-12-00551.1>.
- Mishra, V., Mukherjee, S., Kumar, R. and Stone, D.A. (2017) Heat wave exposure in India in current, 1.5 °C, and 2.0 °C worlds. *Environmental Research Letters*, 12(12), 124012. <https://doi.org/10.1088/1748-9326/aa9388>.
- Morak, S., Hegerl, G.C. and Christidis, N. (2013) Detectable changes in the frequency of temperature extremes. *Journal of Climate*, 26(5), 1561–1574. <https://doi.org/10.1175/JCLI-D-11-00678.1>.
- Nangombe, S., Zhou, T.J., Zhang, W.X., Wu, B., Hu, S., Zou, L.W. and Li, D.H. (2018) Record-breaking climate extremes in Africa under stabilized 1.5 °C and 2 °C global warming scenarios. *Nature Climate Change*, 8(5), 375–380. <https://doi.org/10.1038/s41558-018-0145-6>.
- Oliva, M., Navarro, F., Hrbacek, F., Hernandez, A., Nyvlt, D., Pereira, P., Ruiz-Fernández, J. and Trigo, R. (2017) Recent regional climate cooling on the Antarctic Peninsula and associated impacts on the cryosphere. *Science of the Total Environment*, 580, 210–223. <https://doi.org/10.1016/j.scitotenv.2016.12.030>.
- Otto, F.E.L., Massey, N., van Oldenborgh, G.J., Jones, R.G. and Allen, M.R. (2012) Reconciling two approaches to attribution of the 2010 Russian heat wave. *Geophysical Research Letters*, 39, L04702. <https://doi.org/10.1029/2011GL050422>.
- Pall, P., Aina, T., Stone, D.A., Stott, P.A., Nozawa, T., Hilberts, A.G.J., Lohmann, D. and Allen, M.R. (2011) Anthropogenic greenhouse gas contribution to flood risk in England and Wales in autumn 2000. *Nature*, 470 (7334), 382–385. <https://doi.org/10.1038/nature09762>.
- Paltan, H., Allen, M., Haustein, K., Fuldauer, L. and Dadson, S. (2018) Global implications of 1.5 °C and 2 °C warmer worlds on extreme river flows. *Environmental Research Letters*, 13(9), 094003. <https://doi.org/10.1088/1748-9326/aad985>.
- Perkins, S.E. and Alexander, L.V. (2013) On the measurement of heat waves. *Journal of Climate*, 26(13), 4500–4517. <https://doi.org/10.1175/JCLI-D-12-00383.1>.
- Perkins, S.E., Alexander, L.V. and Nairn, J.R. (2012) Increasing frequency, intensity and duration of observed global heatwaves and warm spells. *Geophysical Research Letters*, 39, L20714. <https://doi.org/10.1029/2012GL053361>.
- Peterson, T.C., Heim, R.R., Hirsch, R., Kaiser, D.P., Brooks, H., Diffenbaugh, N.S., Dole, R. M., Giovannettone, J. P., Guirguis, K., Karl, T. R., Katz, R. W., Kunkel, K., Lettenmaier, D., McCabe, G. J., Paciorek, C. J., Ryberg, K. R., Schubert, S., Silva, V. B. S., Stewart, B. C., Vecchia, A. V., Villarini, G., Vose, R. S., Walsh, J., Wehner, M., Wolock, D., Wolter, K., Woodhouse, C. A. and Wuebbles, D. (2013) Monitoring and understanding changes in heat waves, cold waves, floods, and droughts in the United States: state of knowledge. *Bulletin of the American Meteorological Society*, 94(6), 821–834. <https://doi.org/10.1175/BAMS-D-12-00066.1>.
- Reynolds, J.F., Stafford Smith, D.M., Lambin, E.F., Turner, B.L., Mortimore, M., Batterbury, S.P.J., Downing, T. E., Dowlatabadi, H., Fernández, R. J., Herrick, J. E., Sannwald, E. H., Jiang, H., Leemans, R., Lynam, T., Maestre, F. T., Ayarza, M. and Walker, B. (2007) Global desertification: building a science for dryland development. *Science*, 316(5826), 847–851. <https://doi.org/10.1126/science.1131634>.
- Sanderson, B.M., O'Neill, B.C. and Tebaldi, C. (2016) What would it take to achieve the Paris temperature targets? *Geophysical Research Letters*, 43(13), 7133–7142. <https://doi.org/10.1002/2016GL069563>.
- Sanderson, B.M., Xu, Y.Y., Tebaldi, C., Wehner, M., O'Neill, B., Jahn, A., Pennergrass, A. G., Lehner, F., Strand, W. G., Lin, L., Knutti, R. and Lamarque, J. F. (2017) Community climate simulations to assess avoided impacts in 1.5 °C and 2 °C futures. *Earth System Dynamics*, 8(3), 827–847. <https://doi.org/10.5194/esd-8-827-2017>.
- Scheff, J. and Frierson, D.M.W. (2014) Scaling potential evapotranspiration with greenhouse warming. *Journal of Climate*, 27(4), 1539–1558. <https://doi.org/10.1175/JCLI-D-13-00233.1>.
- Schleussner, C.F., Lissner, T.K., Fischer, E.M., Wohland, J., Perrette, M., Golly, A., Rogelj, J., Childers, K., Schewe, J., Frieler, K., Mengel, M., Hare, W. and Schaeffer, M. (2016) Differential climate impacts for policy-relevant limits to global warming: the case of 1.5 °C and 2 °C. *Earth System Dynamics*, 7(2), 327–351. <https://doi.org/10.5194/esd-7-327-2016>.
- Serreze, M.C. and Stroeve, J. (2015) Arctic sea ice trends, variability and implications for seasonal ice forecasting. *Philosophical Transactions of the Royal Society A: Mathematical Physical and Engineering Sciences*, 373(2045), 20140159. <https://doi.org/10.1098/rsta.2014.0159>.
- Sillmann, J., Kharin, V.V., Zhang, X., Zwiers, F.W. and Bronaugh, D. (2013a) Climate extremes indices in the CMIP5 multimodel ensemble: part 1. Model

- evaluation in the present climate. *Journal of Geophysical Research: Atmospheres*, 118(4), 1716–1733. <https://doi.org/10.1002/jgrd.50203>.
- Sillmann, J., Kharin, V.V., Zhang, X., Zwiers, F.W. and Bronaugh, D. (2013b) Climate extremes indices in the CMIP5 multimodel ensemble: part 2. Future climate projections. *Journal of Geophysical Research: Atmospheres*, 118(6), 2473–2493. <https://doi.org/10.1002/jgrd.50188>.
- Stone, D.A. and Allen, M.R. (2005) The end-to-end attribution problem: from emissions to impacts. *Climatic Change*, 71(3), 303–318. <https://doi.org/10.1007/s10584-005-6778-2>.
- Sui, Y., Lang, X.M. and Jiang, D.B. (2018) Projected signals in climate extremes over China associated with a 2 °C global warming under two RCP scenarios. *International Journal of Climatology*, 38, E678–E697. <https://doi.org/10.1002/joc.5399>.
- Vose, R.S., Easterling, D.R. and Gleason, B. (2005) Maximum and minimum temperature trends for the globe: an update through 2004. *Geophysical Research Letters*, 32(23), L23822. <https://doi.org/10.1029/2005GL024379>.
- Wang, K.C. and Dickinson, R.E. (2013) Contribution of solar radiation to decadal temperature variability over land. *Proceedings of the National Academy of Sciences of the United States of America*, 110(37), 14877–14882. <https://doi.org/10.1073/pnas.1311433110>.
- Wang, Z.L., Lin, L., Zhang, X.Y., Zhang, H., Liu, L.K. and Xu, Y.Y. (2017) Scenario dependence of future changes in climate extremes under 1.5 °C and 2 °C global warming. *Scientific Reports*, 7, 46432. <https://doi.org/10.1038/srep46432>.
- Wild, M., Folini, D., Schar, C., Loeb, N., Dutton, E.G. and Konig-Langlo, G. (2013) The global energy balance from a surface perspective. *Climate Dynamics*, 40(11–12), 3107–3134. <https://doi.org/10.1007/s00382-012-1569-8>.
- Xing, W., Wang, B. and Yim, S.Y. (2016) Peak-summer East Asian rainfall predictability and prediction, part I: Southeast Asia. *Climate Dynamics*, 47 (1–2), 1–13. <https://doi.org/10.1007/s00382-014-2385-0>.
- You, Q.L., Kang, S.C., Aguilar, E., Pepin, N., Flugel, W.A., Yan, Y.P., Xu, Y. W., Zhang, Y. J. and Huang, J. (2011) Changes in daily climate extremes in China and their connection to the large scale atmospheric circulation during 1961–2003. *Climate Dynamics*, 36(11–12), 2399–2417. <https://doi.org/10.1007/s00382-009-0735-0>.
- You, Q.L., Jiang, Z.H., Wang, D., Pepin, N. and Kang, S.C. (2018) Simulation of temperature extremes in the Tibetan Plateau from CMIP5 models and comparison with gridded observations. *Climate Dynamics*, 51(1–2), 355–369. <https://doi.org/10.1007/s00382-017-3928-y>.
- Zhang, X.B., Alexander, L., Hegerl, G.C., Jones, P., Tank, A.K., Peterson, T.C., Trewin, B. and Zwiers, F. W. (2011) Indices for monitoring changes in extremes based on daily temperature and precipitation data. *Climatic Change*, 2(6), 851–870. <https://doi.org/10.1002/wcc.147>.
- Zhou, T.J. and Zou, L.W. (2010) Understanding the predictability of East Asian summer monsoon from the reproduction of land–sea thermal contrast change in AMIP-type simulation. *Journal of Climate*, 23(22), 6009–6026. <https://doi.org/10.1175/2010JCLI3546.1>.

How to cite this article: Zhang M, Yu H, Huang J, Wei Y, Liu X, Zhang T. Comparison of extreme temperature response to 0.5 °C additional warming between dry and humid regions over East-central Asia. *Int J Climatol*. 2019;39:3348–3364. <https://doi.org/10.1002/joc.6025>